Ceramics International 44 (2018) 17440–17446

Contents lists available at ScienceDirect

Ceramics International

journal homepage: www.elsevier.com/locate/ceramint

# Dopant-dependent diffusion behavior of SiAlON ceramics against Inconel 718 superalloy

Ali Çelik

*Bilecik Şeyh Edebali University, Department of Metallurgical and Materials Engineering, Bilecik, Turkey*

ARTICLE INFO

*Keywords:*
SiAlON
Rare-earth
Diffusion
Inconel 718
Microscopy

ABSTRACT

The utilization of SiAlON ceramics at high speed machining of superalloys has been increasing day by day. In these operations, chemical wear, based on diffusion of tool and work-piece atoms towards each other due to high temperature and pressure at the cutting zone, is the dominant tool failure mechanism. In this study, dopant-dependent diffusion behavior of SiAlON ceramics, prepared by using different rare-earth elements (Y, Yb, Er and Ce), against Inconel 718 alloy was investigated. The SiAlON-Inconel 718 diffusion couples were manufactured by SPS technique. It was observed that the diffusion zone thickness was strongly dependent on the type of the rare-earth used in the composition and Er-doped SiAlON samples had a higher interaction zone in comparison to the others. Moreover, crystallization of grain boundary phase was observed as an effective parameter on the zone thickness for Er-doped compositions.

## 1. Introduction

SiAlON is one of the most important structural ceramics for various applications such as attrition milling arms, wire extrusion dies, roll bearings, cutting tools etc. in which high wear resistance, physical and chemical stability, high temperature durability and thermal shock resistance are required [1]. The cutting tools utilized for high speed turning and milling of nickel based aerospace alloys are good examples for these challenging applications.

As being one of the most widely used superalloys, Inconel 718 exhibits excellent mechanical strength and creep resistance at elevated temperatures and is defined as “difficult to cut material” due to its superior high temperature properties. Many studies were reported over decades in order to explain cutting performance of SiAlON tools on turning of Inconel 718. Zheng et al. [2] studied wear mechanisms during high speed turning of Inconel 718 alloy with SiAlON cutting tools and found that main wear mechanisms were adhesive and abrasive wear. Zhuang et al. [3] investigated the correlation between notch wear at the cutting edge of SiAlON based turning inserts and work hardened layer formed on the surface of Inconel 718 alloy during turning experiments conducted at a cutting speed of 200 m/min. Their results showed that the depth of the notch wear was directly proportional to the hardened layer beneath the machined surface. Altin et al. [4] analyzed wear mechanisms of SiAlON and SiC whisker reinforced alumina inserts depending on cutting speed. The authors concluded that diffusion based wear mechanisms such as notch, adhesion and crater wear were dominant at high cutting speeds (200–300 m/min), whereas flank wear and thermal cracking were the main wear mechanisms at relatively low cutting speeds (< 200 m/min.).

Although, SiAlON based ceramics have been studied extensively in high-speed turning of Inconel 718, there are limited number of study on utilization of SiAlON based ceramics at high-speed milling of superalloys. Zheng et al. [5] investigated relative cutting performance of graded nano-ceramic round inserts based on $Si_3N_4$/TiCN and commercial $Al_2O_3$-$SiC_w$ ceramic tools on ultra-high speed milling of Inconel 718. They observed micro-chipping, microcracking, abrasion and adhesion as the main wear mechanisms on the cutting edges of the tools. Tian et al. [6] studied high-speed face-milling of Inconel 718 with SiAlON ceramic tools under dry cutting conditions. While the notch wear was found to be the dominant mechanism when the cutting speed is relatively low (600–1400 m/min.), the dominant wear mechanism turned into adhesion wear at the cutting edges of the tools at higher cutting speeds in the range of 1800–3000 m/min. In another study performed by Akhtar et al. [7], surface integrity of Inconel 718 alloy, which was high speed milled by coated carbide and ceramic inserts, was analyzed. The authors observed that finish surface roughness of the work-piece alloy, machined with whisker reinforced alumina tool was lower than that of the alloy machined with coated carbide tool due to the adherence of material debris at higher cutting speeds at which the ceramic tool was tested. In a recent study, Çelik et al. [8] manufactured and tested a novel α/β-SiAlON solid milling tool and its TiN reinforced composite on high speed milling of Inconel 718. A severe adhesion of work piece material to the cutting edge and a subsequent crater formation due to removal of the adhered layer from the cutting edge was

*E-mail address:* ali.celik@bilecik.edu.tr.

https://doi.org/10.1016/j.ceramint.2018.06.211
Received 21 May 2018; Received in revised form 7 June 2018; Accepted 25 June 2018
Available online 26 June 2018

observed under dry cutting conditions.

As stated in the literature on high speed cutting of superalloys with SiAlON cutting materials, adhesive and a subsequent chemical wear, based on the interaction of the tool and work-piece atoms, are responsible for tool failure during high speed machining of superalloys at elevated temperatures. Therefore, it is critical to understand the effective parameters on the chemical resistance of SiAlON ceramics against softened Inconel 718 alloy. In this study, it was aimed to investigate diffusion behavior between Inconel 718 and SiAlON ceramics that contain different rare-earth dopants, which is one of the most effective parameters on the performance of the material, in order to elucidate wear behavior of SiAlON based cutting tools. The diffusion couples of SiAlON-Inconel 718 were manufactured by a novel technique based on heating and pressing of sandwiched samples in a spark plasma sintering (SPS) furnace, simultaneously and examined by scanning electron microscope (SEM) and an attached energy dispersive x-ray (EDX) detector.

## 2. Materials and methods

The experimental part of this study was divided into three sections as manufacturing of SiAlON ceramics with different rare-earth dopants, production of SiAlON-Inconel 718 diffusion couples by SPS and microstructural characterization of sintered SiAlONs and diffusion couples.

### 2.1. Production of SiAlON ceramics

A Y-Sm-Ca multi-cation doped α/β-SiAlON, the cutting performance of which was investigated by Çelik et al. [8] and labelled as S-YSC, was considered as the reference composition in this study. Three compositions were derived from S-YSC by replacing the main dopant, Y, with Yb, Er and Ce and designated as S-YbSC, S-ErSC and S-CeSC, respectively. Two other compositions, which contain single dopant (100 mol% of Y and Er), were designed to determine the effect of Sm and Ca in the dopant system on diffusion scale at the interface of SiAlON-Inconel 718 and labelled as S-Y and S-Er.

SiAlON compositions were prepared by wet mixing and milling of raw powders $Si_3N_4$ (UBE-SE10/Japan), AlN (Tokuyama/Japan), $Al_2O_3$ (Sumitomo/Japan), $Y_2O_3$ (Treibacher/Austria), $Yb_2O_3$ (Treibacher/Austria), $Er_2O_3$ (Treibacher/Austria), $CeO_2$ (Treibacher/Austria), $Sm_2O_3$ (Treibacher/Austria), (Treibacher/Austria) and CaO (in the form of $CaCO_3$), in an attrition mill (Union Process/USA) with a spindle speed of ~ 600 rpm for 2 h. The sluries were then further mixed for an additional 1 h after addition of organic pressing additives in the amount of ~ 6 wt%. After an efficient mixing step, the slurries were converted to the SiAlON granules with an average diameter of 100 μm and humidity of < 1% by means of a spray dryer. Cold isostatic pressing was performed by compacting the granules in a flexible mold at a hydrostatic pressure of 200 MPa to obtain green cylindirical samples. A low temperature heat treatment (~ 600 °C) was applied to remove pressing additives prior to sintering. Then, the green samples were sintered at 1900 °C for 1 h soaking time under $N_2$ gas pressure in a gas pressure sintering (GPS) furnace (FCT-Anlagenbau GmbH).

### 2.2. Production of SiAlON-Inconel 718 diffusion couples

The chemical composition of Inconel 718 superalloy, determined by EDX analysis is given in Table 1. The diffusion couples were formed by sandwiching a piece of square Inconel 718 alloy with a dimension of 5 × 5 × 3 mm between two cylindrical SiAlON pellets with a diameter and a thickness of 12 and 5 mm, respectively. The SiAlON pellets and Inconel 718 alloy were placed into a graphite mold setup as shown schematically in Fig. 1. The sandwiched Inconel 718 and SiAlON materials were heated and pressed under vacuum condition between the rams of SPS furnace (FCT Systeme GmbH), simultaneously. The samples, in surface contact, was kept at the maximum operating temperature of 1200 °C for 30 min in order to allow diffusion to take place at their interfaces. The configuration of SPS furnace, the operating conditions of SPS process and a representative picture of the cross-section of a diffusion couple are given in Fig. 1.

**Table 1**
The composition of the Inconel 718 superalloy.

| | C | Al | Ti | Cr | Fe | Nb | Mo | Ni |
|---|---|---|---|---|---|---|---|---|
| wt% | 4.32 | 4.42 | 0.76 | 15.26 | 18.33 | 3.60 | 2.35 | Balance |

### 2.3. Characterization of materials

Microstructures of the sintered SiAlON ceramics and the interfaces of the SiAlON-Inconel 718 diffusion couples were examined by SEM (Zeiss-Supra 50VP) and an energy dispersive X-ray spectroscopy (EDX) attached to this microscope. Phase analysis of the SiAlON ceramics and $z$ value of the β-SiAlON, which indicates the solubility of Al and O in general formula of $\beta\text{-}Si_{6-z}Al_zO_zN_{8-z}$, were determined by a X-ray diffractometer (XRD) (Rigaku-Miniflex 600). The XRD samples prepared by mixing of SiAlON powder with a reference Si powder (~ 10 wt%), then the measurements were carried out with a scan speed of 0,2°/min. for the 2θ values between 25° and 40°. The relative proportions of α and β-SiAlON phases were calculated by using the intensities of the (102) and (210) diffraction peaks for hexagonal α-SiAlON and (101) and (210) peaks for β-SiAlON crystals as follows:

$$\frac{I_\beta}{I_\beta + I_\alpha} = \frac{1}{1+\kappa[(1/w_\beta)-1]} \quad (1)$$

where $I_\alpha$ and $I_\beta$ are the intensities of α and β-SiAlON peaks, respectively, $w_\beta$ is the relative weight fraction of β-SiAlON, and κ is a constant that equals to 0.518 for β (101) − α (102) reflections and 0.544 for β (210) − α (210) reflections [9]. The $z$ value of β phase was calculated by taking the average of $z_a$ and $z_c$, which were calculated by the Eqs. (2) and (3) given as follow:

$$z_a = \frac{a-7.6044}{0.031} \quad (2)$$

$$z_c = \frac{c-2.9075}{0.026} \quad (3)$$

where $a$ and $c$ are the calculated dimensions of β-SiAlON hexagonal unit cell.

## 3. Results and discussion

### 3.1. Microstructural characterization of SiAlON ceramics

It is supposed that the interaction behavior of SiAlON ceramics with Inconel 718 strongly depends on the composition and microstructural characteristics of materials, as well as the manufacturing conditions of the diffusion couples that are listed in Fig. 1. Fig. 2 shows the back scattered electron (BE) images of the SiAlON ceramics after GPS at 1900 °C and 100 bar maximum temperature and pressure, respectively. While, β-SiAlON phase is observed as dark gray rod-like grains, α-SiAlON phase appears as more brighter and equiaxed grains due to partial solubility of high atomic number rare earth atoms in α-$Si_3N_4$ crystal lattice. The sub-micron size white islands distributed throughout the microstructure are the grain boundary oxynitride crystalline/amorphous phase mainly composed of the elements of the rare-earth oxides, silicon and nitrogen. It can be clearly seen in Fig. 2 that microstructural characteristics of the SiAlON ceramics were strongly affected by the type of the rare-earth dopant. A similar microstructure for S-YSC, S-YbSC and S-ErSC compositions in terms of grain shape, size and amount of α and β-SiAlON phases was observed (Fig. 2(a), (b), and

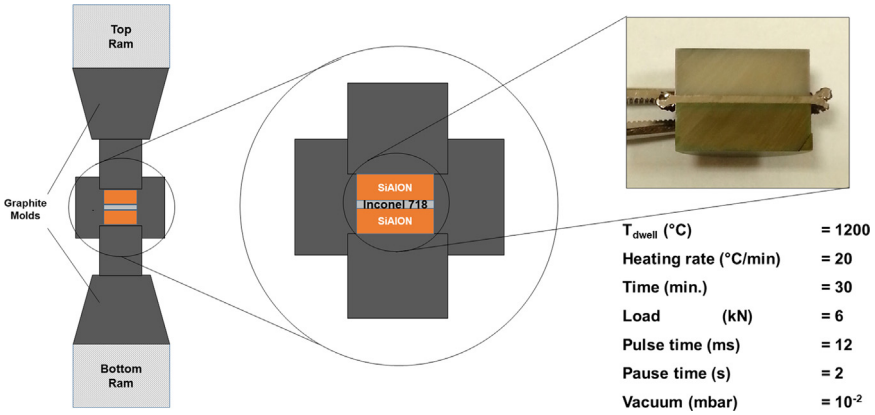


**Fig. 1.** Schematic illustration and operating conditions of SPS furnace used for manufacturing of diffusion couples.

(c), respectively). On the other hand, a more bimodal microstructure with large β-SiAlON grains surrounded by much finer α or β-SiAlON grains, was obtained for the $Ce^{+2}$-doped S-CeSC composition (Fig. 2. d). Furthermore, large α-SiAlON grains that were observed in the microstructures of S-YSC, S-YbSC, S-ErSC and S-Er samples were not detected in the microstructure of $Ce^{+2}$-doped sample, proving that the stabilization of α-SiAlON phase is constrained by $Ce^{+2}$ in comparison to the other rare earth elements. According to Ekstrom [10], the largest rare-earth cation to be able to enter the α-SiAlON structure alone is $Nd^{3+}$, with an ionic radius of 0.98 Å. The larger cations such as $La^{3+}$ ($r = 1.03$ Å) and $Ce^{3+}$ ( = 1.01 Å) are considered unable to occupy alone the interstitial sites in α-SiAlON crystal structure. One way to incorporate $Ce^{+2}$ atoms into α-SiAlON structure was reported as the utilization of $Ce^{+2}$ together with smaller rare earth cations, such as $Y^{+3}$, $Yb^{+3}$, etc. [11,12]. In this study, 5 mol% of $Sm^{3+}$ and $Ca^{2+}$ (with a radius of 0.958 and 1 Å, respectively) were used together with $Ce^{+2}$. However, stabilization of α-phase was not achieved for this composition due to their insufficient amounts as confirmed by the results of XRD analysis shown in Fig. 3. The characteristic peaks of α-SiAlON phase at 2θ values of 30.8°, 34.2° and 35.2° were not observed in the corresponding spectra. Although small amount of $Sm^{+3}$ and $Ca^{+2}$ in S-CeSC composition were ineffective on the stabilization of α-SiAlON phase, their effects were much more obvious for $Y^{+3}$ and $Er^{+3}$ doped compositions. A strong crystallization of grain boundary phase in the form of melilite with a general formula of $Ln_2Si_{3-x}Al_xO_{3+x}N_{4-x}$ was detected due to the absence of these cations for $Er^{+3}$ and $Y^{+3}$ doped

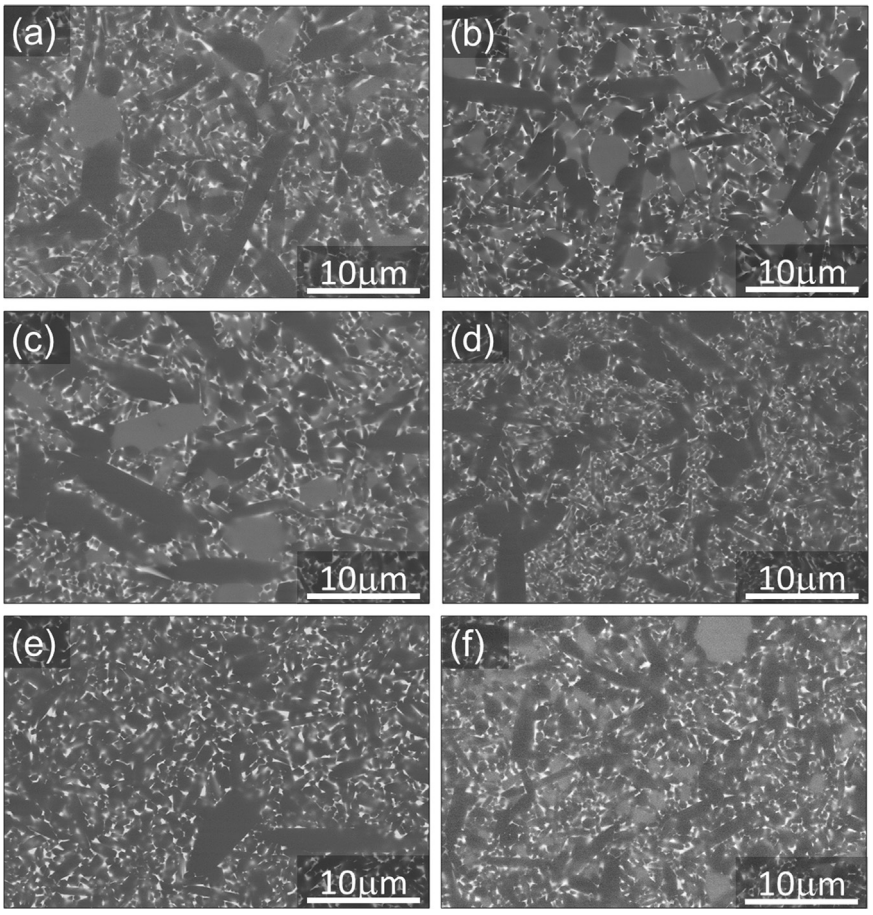


**Fig. 2.** BE-SEM micrographs of (a) S-YSC, (b) S-YbSC, (c) S-ErSC, (d) S-CeSC, (e) S-Y and (f) S-Er compositions.

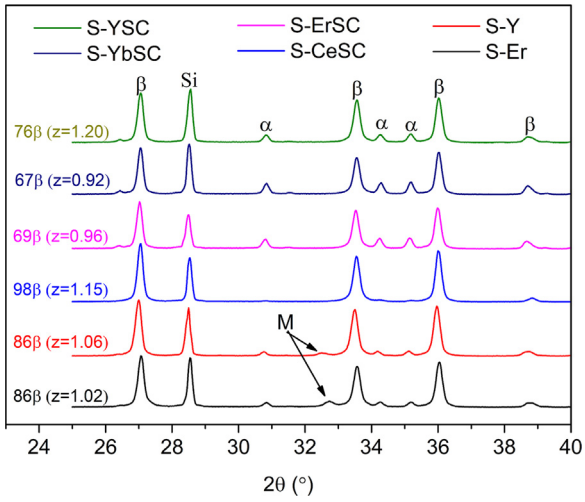


**Fig. 3.** XRD spectra of SiAlON samples with different dopant type.

samples (Fig. 3). Moreover, using $Er^{+3}$ as a single dopant in S-Er resulted in elimination of large α-SiAlON grains, as well as a reduction in number of large β-SiAlON grains, as shown in Fig. 2(e) and (f). Therefore, a monomodal microstructure with a lower amount of α-SiAlON and crystalline grain boundary phases was obtained. While the same α/β-SiAlON ratio is maintained, a reduction of overall grain size was also observed for S-Y sample. The change in the ratio of α/β-SiAlON, grain growth and crystallization of grain boundary phase most probably arises from variations in viscosities of the RE-rich liquid phases during sintering as suggested by Zenotchkine et al. [13], Kleebe [14], Cao and Metselaar [15] and Mandal [16].

$Al_2O_3$ solubility in the crystal structure of β-SiAlON, indicated by $z$ value, plays an important role on mechanical behavior of SiAlON based ceramics [17,18]. As shown in Fig. 3, a negligible difference in the $z$ values of β-SiAlON phase depending on the type of RE used in compositions, were calculated. Therefore, the effect of $z$ value of β-SiAlON on chemical properties of α/β-SiAlON ceramics as was neglected.

### 3.2. Comparison of diffusion scales of SiAlON ceramics

In order to reveal the chemical interaction between SiAlON based ceramics and Inconel 718 without performing high speed machining tests, at which high chemical wear occurs at the cutting zone due to high temperature and pressure are exerted on tool materials, diffusion couples were manufactured with a novel SPS technique. Fig. 4 shows the microstructures of the interaction zone between SiAlON and Inconel718, with a total thickness varying between 10 and 15 μm. While S-YSC, S-YbSC and S-CeSC samples had a similar zone thickness about ~ 10 μm, a considerable difference in the interaction zone thickness was measured (~ 15 μm) for $Er^{+3}$ doped S-ErSC composition. By considering the similar α/β-phase ratio of S-ErSC and S-YbSC compositions given in Fig. 3, it can be concluded that there is not a direct correlation between α/β phase ratio and diffusion zone thickness. This was also confirmed by the moderate zone thickness of S-CeSC composition (11.16 μm), which was almost lack of α-SiAlON phase. Another inconsistent behavior on diffusion zone thicknesses was observed in case of single-doped S-Y and S-Er compositions. The β-SiAlON content was increased by 10% and 19% for $Y^{+3}$ and $Er^{+3}$-doped systems, respectively, as the result of a change in the dopant system from multi to single for these compositions. However, the diffusion zone thickness of $Y^{+3}$-doped system was not affected by the absence of $Sm^{+3}$ and $Ca^{+2}$, while it was slightly decreased when there is no other dopants in the $Er^{+3}$ system. Therefore, the decrease in the zone thickness of the $Er^{+3}$ system was attributed to the crystallinity of grain boundary phase as nitrogen-melilite (Fig. 3). Chee et al. [19] were suggested that nitrogen-melilite (containing 67 eq.% of nitrogen) is an attractive grain boundary phase for high temperature performance of SiAlON ceramics due to its high refractoriness. Crystallization of melilite phase at the grain boundaries of $Er^{+3}$ and $Y^{+3}$ doped SiAlON ceramics was also reported by Bandyopadhyay et al. [20] and Ijevskii et al. [21].

A representative EDX analyses in mapping mode showing the distribution of the elements at the interface of S-YSC/Inconel718 is given in Fig. 5. A Nb and Mo rich region (Fig. 5(c) and (d)) was observed as a slightly brighter layer adjacent to the Inconel 718 side in BE image (Fig. 5(a)). Nb, as a main former of γ', γ'' and δ phases in Inconel 718 [22], was also detected at the boundary of SiAlON-diffusion zone as shown in Fig. 5(c). Between these Nb-rich layers, a relatively high Al concentration was observed as a porosity-like dark regions (Fig. 5(a)) which were distributed in a matrix composed mainly of Cr, Mo and Ni elements according to the Fig. 5(b), (d) and (f), respectively. The thickness of this particulate composite structure was about 2–3 μm. Although, Al presents in both SiAlON and Inconel 718 side, the Al-rich grains were supposed to be formed as the result of the diffusion of Al atoms from Inconel 718 to SiAlON due to high stability of Al in the form of $Al_2O_3$, which was reported by Peteves [23] and Chakraborty et al. [24] as − 1155 kJ/g mole at 1200 °C. Moreover, Al was expressed as a critical component in diffusion process since the Al-O bonds in SiAlON structure acts as a barrier for the diffusion of atoms from metal side [24,25]. In this case, the size and the amount of Al rich grains distributed to the diffusion zones of the SiAlON ceramics was found quite similar to each other (Fig. 4). Therefore, Al-rich grains were not taken under consideration as a parameter, which affected the resultant diffusion scale thicknesses. The last characteristic layer adjacent to SiAlON side was distinguished as dark gray region, in which Nb as well as Cr, Ni, Mo and Fe concentrations are relatively high according to the corresponding EDX maps given in Fig. 5(b) to (f). While Nb-rich layer was much more explicit in the microstructure of S-ErSC and S-CeSC samples (Fig. 4(c) and (d), respectively), it was observed as more discontinous for the other compositions. It should be also noted that the concentration of Si at the interface was approximately zero indicating that Si, as well as N, diffused towards the metal alloy with a relatively high diffusion rate. The high diffusion rates of Si and N from ceramic to metal are in agreement with the results of Chakraborty et al. [24], who investigated the diffusion behavior between $Si_3N_4$ and a stainless steel with a grade of 304 L.

If necessary to summarize, the diffusion zone between SiAlON ceramics and Inconel 718 alloy had three characteristic sub-layers in terms of microstructure and composition of the diffused elements as schematically illustrated in Fig. 6. While first layer was observed as a bright Nb-rich layer adjacent to the Inconel 718 side, the third layer was seen as dark gray region in which Cr, Ni, Mo and Fe as well as Nb concentrations were high. Between these two layers, a particulate composite-like structure forming the second layer was detected. High Al concentration was found in particle like phases, which were surrounded by a matrix containing Cr, Ni and Mo elements.

## 4. Conclusions

In this study, dopant-dependent diffusion behavior of SiAlON ceramics, prepared by using different rare-earth elements (Y, Yb, Er and Ce), against Inconel 718 alloy was investigated. The SiAlON-Inconel 718 diffusion couples were manufactured by SPS technique. Accordingly, the following conclusions were drawn:

- In case of using $Ce^{+2}$ as a main dopant in the composition, the stabilization of α-SiAlON phase was not achieved due to high ionic radius of $Ce^{+2}$. Utilizing $Er^{+3}$ and $Y^{+3}$ as single dopant altered the final composition and microstructure. While the growth of rod-like β-SiAlON grains was inhibited due to absence of $Sm^{+3}$ and $Ca^{+2}$, the amount of α-SiAlON phase decreased in both $Y^{+3}$ and $Er^{+3}$ systems.

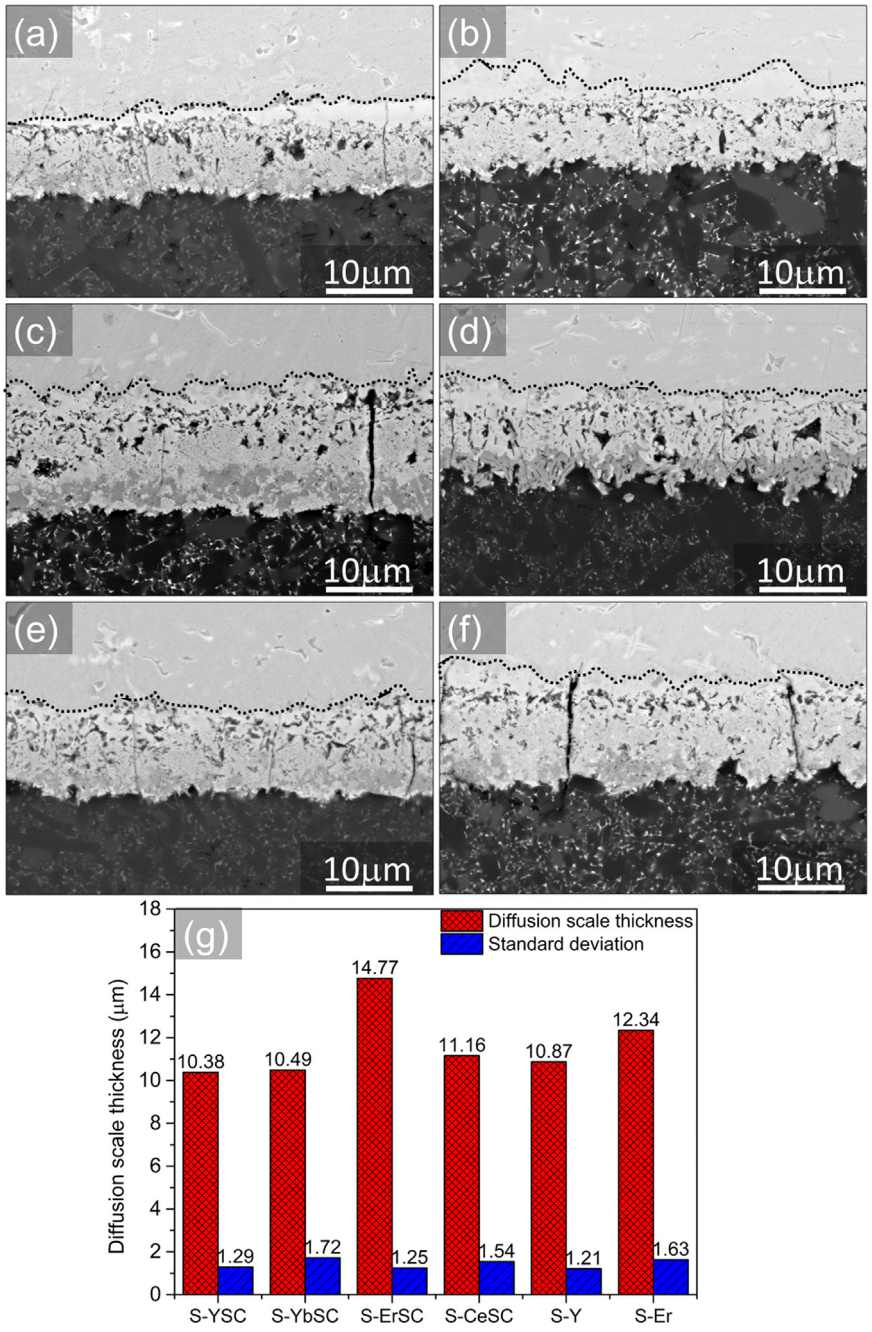


**Fig. 4.** BE-SEM micrographs of the diffusion interfaces of (a) S-YSC, (b) S-YbSC, (c) S-ErSC, (d) S-CeSC, (e) S-Y, (f) S-Er, and (g) the thickness of the diffusion zones of these compositions.

- $Er^{+3}$-doped compositions (S-ErSC and S-Er) exhibited a higher diffusion zone thickness in comparison to the other compositions, the diffusion zone thicknesses of which are quite similar to each other (10–11 μm). It was concluded that there was not a direct correlation between the diffusion zone thickness and α/β-SiAlON phase ratio by considering the similar α/β-phase ratio of S-ErSC and S-YbSC compositions. This was also confirmed by the moderate zone thickness of S-CeSC composition, which was almost lack of α-SiAlON phase. The considerable reduction in the diffusion zone thickness due to change in dopant system from multi to single was believed as the result of strong crystallization of the grain boundary phase as melilite in case of $Er^{+3}$ system.
- It was found that the diffusion zone between SiAlON ceramics and Inconel 718 alloy had three characteristic sub-layers in terms of microstructure and composition of the diffused elements. While first layer was observed as a bright Nb-rich layer adjacent to the Inconel 718 side, the third layer was seen as dark gray region in which Cr, Ni, Mo and Fe as well as Nb concentrations were high. Between these two layer, Al-rich particulates surrounded by a matrix containing Cr, Ni and Mo elements.
- Since high speed machining is a dynamic process in which the chip is always in a continuous sliding movement on the rake faces of the tool, the chemical wear resistance of α/β-SiAlON ceramics during high speed machining of Inconel 718 is proposed to be dependent not only on the ease of formation of the diffusion products, but also on their integrity to the SiAlON substrate under thermal and mechanical stresses, which was directly related to the compatibility of coefficients of thermal expansion.

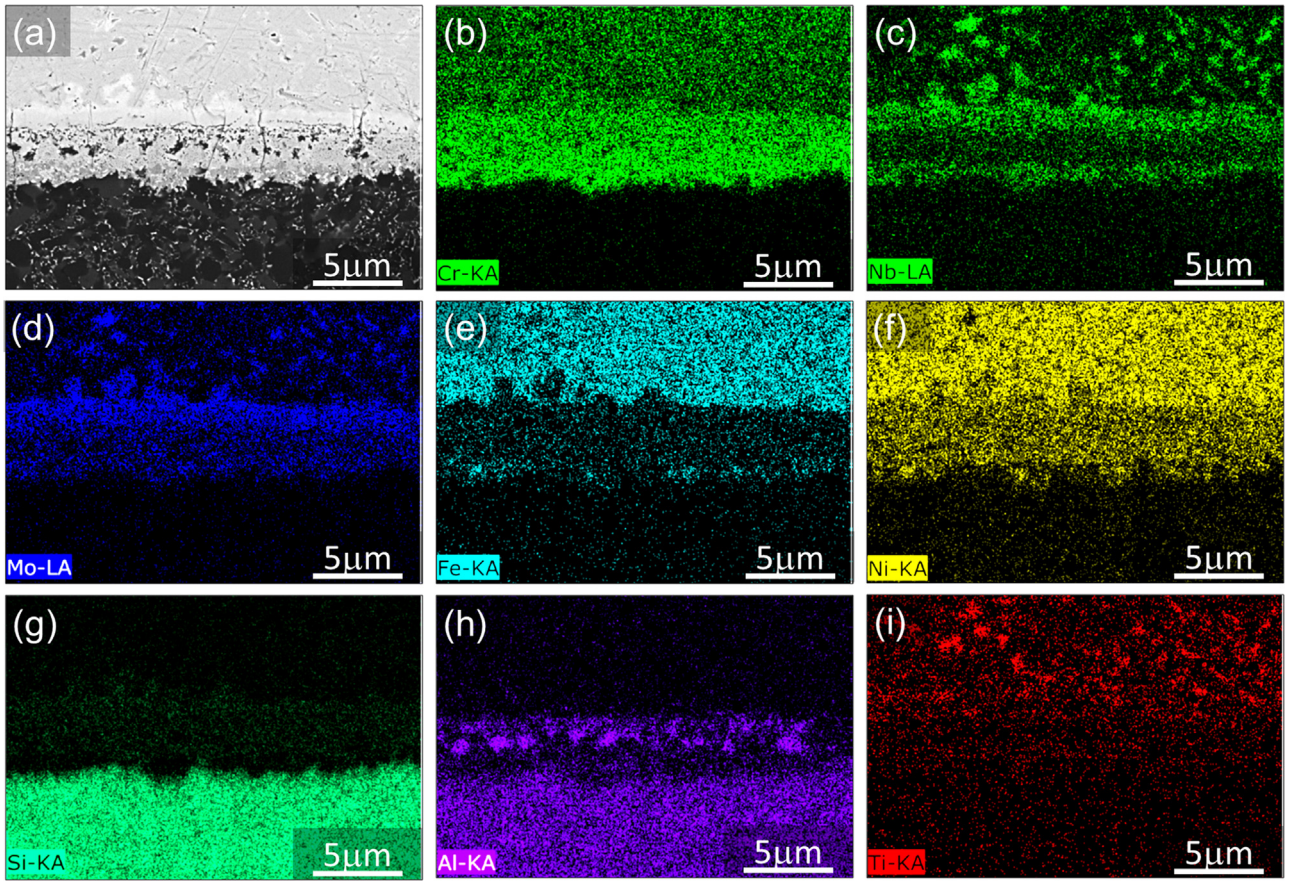


**Fig. 5.** (a) BE-SEM micrograph and EDX mapping results showing the distribution of (b) Cr, (c) Nb, (d) Mo, (e) Fe, (f) Ni, (g) Si, (h) Al and (i) Ti in the diffusion zone of S-YSC sample.

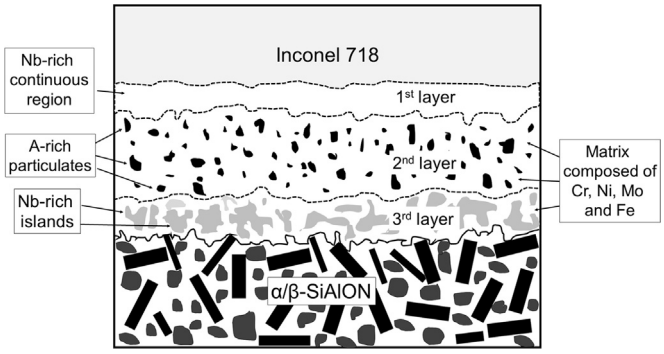


**Fig. 6.** Schematic illustration of the structure of diffusion interface between SiAlON and Inconel 718 alloy.

## Acknowledgements

The financial support for this study by Bilecik Seyh Edebali University Scientific Research Projects Commission (under the project numbers of 2016-02.BŞEÜ.03-10) is gratefully acknowledged. The author also thanks to the Head of Materials Science and Engineering Department, Anadolu University for facilitating SPS experiments and MDA Co Inc. for kindly providing raw powders.

## References

[1] A. Çelik, I. Lazoglu, A. Kara, F. Kara, Wear on SiAlON ceramic tools in drilling of aerospace grade CFRP composites, Wear 338 (2015) 11–21.
[2] G.M. Zheng, J. Zhao, X.Y. Song, C.Q. Yan, Y.E. Li, Ultra high speed turning of Inconel 718 with SiAlON ceramic tools, Adv. Mater. Res. 126–128 (2010) 653–657.
[3] K. Zhuang, D. Zhu, X. Zhang, H. Ding, Notch wear prediction model in turning of Inconel 718 with ceramic tools considering the influence of work hardened layer, Wear 313 (1–2) (2014) 63–74.
[4] A. Altin, M. Nalbant, A. Taskesen, The effects of cutting speed on tool wear and tool life when machining Inconel 718 with ceramic tools, Mater. Des. 28 (9) (2007) 2518–2522.
[5] G. Zheng, J. Zhao, Y. Zhou, A. Li, X. Cui, X. Tian, Performance of graded nano-composite ceramic tools in ultra-high-speed milling of Inconel 718, Int. J. Adv. Manuf. Technol. 67 (9–12) (2013) 2799–2810.
[6] X. Tian, J. Zhao, J. Zhao, Z. Gong, Y. Dong, Effect of cutting speed on cutting forces and wear mechanisms in high-speed face milling of Inconel 718 with SiAlON ceramic tools, Int. J. Adv. Manuf. Technol. 69 (9–12) (2013) 2669–2678.
[7] W. Akhtar, J. Sun, W. Chen, Effect of machining parameters on surface integrity in high speed milling of super alloy GH4169/Inconel 718, Mater. Manuf. Process. 31 (5) (2016) 620–627.
[8] A. Çelik, M.S. Alağaç, S. Turan, A. Kara, F. Kara, Wear behavior of solid SiAlON milling tools during high speed milling of Inconel 718, Wear 378 (2017) 58–67.
[9] K. Liddell, X-ray Analysis of Nitrogen Ceramic Phases (MSc thesis), University of Newcastle, Upon Tyne, UK, 1979.
[10] T. Ekström, M. Nygren, SiAlON ceramics, J. Am. Ceram. Soc. 75 (2) (1992) 259–276.
[11] H. Mandal, New developments in α-SiAlON ceramics, J. Eur. Ceram. Soc. 19 (13–14) (1999) 2349–2357.
[12] H. Yurdakul, S. Turan, The valance determination of cerium ions in α-SiAlON by electron energy loss spectroscopy analysis, Microsc. Microanal. 14 (S3) (2008) 19–22.
[13] M. Zenotchkine, R. Shuba, I.W. Chen, Liquid-phase growth of small crystals for seeding α-SiAlON ceramics, J. Am. Ceram. Soc. 87 (6) (2004) 1040–1046.
[14] H.J. Kleebe, G. Pezzotti, G. Ziegler, Microstructure and fracture toughness of $Si_3N_4$ ceramics: combined roles of grain morphology and secondary phase chemistry, J. Am. Ceram. Soc. 82 (7) (1999) 1857–1867.
[15] G.Z. Cao, R. Metselaar, G. Ziegler, Relations between composition and micro-structure of SiAlONs, J. Eur. Ceram. Soc. 11 (2) (1993) 115–122.
[16] H. Mandal, D.P. Thompson, T. Ekström, Reversible α⇌ SiAlON transformation in heat-treated SiAlON ceramics, J. Eur. Ceram. Soc. 12 (6) (1993) 421–429.
[17] P.F. Becher, E.Y. Sun, K.P. Plucknett, K.B. Alexander, C.H. Hsueh, Microstructural design of silicon nitride with improved fracture toughness: I. Effects of grain shape and size, J. Am. Ceram. Soc. 81 (11) (1998) 2821–2830.
[18] E.Y. Sun, P.F. Becher, K.P. Plucknett, C.H. Hsueh, K.B. Alexander, S.B. Waters, Microstructural design of silicon nitride with improved fracture toughness: ii.

Effects of yttria and alumina additives, J. Am. Ceram. Soc. 81 (11) (1998) 2831–2840.
[19] K.S. Chee, Y.B. Cheng, M.E. Smith, The solubility of aluminium in rare earth nitrogen melilite phases, J. Eur. Ceram. Soc. 15 (12) (1995) 1213–1220.
[20] S. Bandyopadhyay, M.J. Hoffmann, G. Petzow, Densification behavior and properties of $Y_2O_3$-containing α-SiAlON-based composites, J. Am. Ceram. Soc. 79 (6) (1996) 1537–1545.
[21] V.A. Ijevskii, U. Kolitsch, H.J. Seifert, I. Wiedmann, F. Aldinger, Aluminum-containing ytterbium nitrogen woehlerite solid solutions; Synthesis, structure, and some properties, J. Eur. Ceram. Soc. 18 (5) (1998) 543–552.
[22] C. Slama, M. Abdellaoui, Structural characterization of the aged Inconel 718, J. Alloy. Compd. 306 (1–2) (2000) 277–284.
[23] S.D. Peteves, Joining nitride ceramics, Ceram. Int. 22 (6) (1996) 527–533.
[24] G. Chakraborty, S. Bandyopadhyay, B. Haldar, R. Das, Diffusion phenomena in the α-$Si_3N_4$-solid solution and 304L stainless steel static interaction couple, Ceram. Int. 37 (3) (2011) 1011–1016.
[25] J.A. Yeomans, T.F. Page, Studies of ceramic-liquid metal reaction interfaces, J. Mater. Sci. 25 (5) (1990) 2312–2320.